AUTOMATIC ANALYSIS OF LEFT VENTRICLE WALL THICKNESS USING SHORT-AXIS CINE CMR IMAGES

F. Khalifa[1], *G. M. Beache*[2], *M. Nitzken*[1], *G. Gimel'farb*[3], *G. Giridharan*[4], *and A. El-Baz*[1]*

[1]BioImaging Laboratory, Bioengineering Department,University of Louisville, Louisville, KY, USA.
[2]Diagnostic Radiology Department, School of Medicine, University of Louisville, Louisville, KY, USA.
[3]Department of Computer Science, University of Auckland, Auckland, New Zealand.
[4]Bioengineering Department, University of Louisville, Louisville, KY, USA.

ABSTRACT

A new automatic framework for analyzing wall thickness and thickening function on short-axis cine cardiac magnetic resonance (CMR) images is proposed. Inner and outer wall borders (contours) are segmented in a CMR image with a level set deformable model. Its evolution is controlled by a stochastic speed function that accounts for an "object-background" Markov-Gibbs shape and appearance model. Found by solving a Laplace equation, point-to-point correspondences between the inner and outer borders provide initial estimates of the local wall thickness and thickening function index. Effects of segmentation errors are reduced and a 3-D continuity analysis of the left ventricle (LV) wall thickening values is performed by using the maximum *a posteriori* (MAP) estimates for a pairwise energy function of a generalized Gauss-Markov random field (GGMRF) probabilistic model. Experiments with *in vivo* CMR data confirm the robustness and accuracy of the proposed framework.

Index Terms— Wall thickness analysis, Regional myocardium function, Level set, Markov–Gibbs random field, Laplace equation.

1. INTRODUCTION

Measuring wall thickness throughout the cardiac cycle in cardiac magnetic resonance (CMR) images provides key local information for deriving integrated physiological parameters of an individual in health and disease [1]. To reliably measure the wall thickness and assess the left ventricle (LV) thickening, one has to accurately segment inner and outer wall boundaries in the CMR images.

Most successful known approaches have addressed the challenge by modeling object appearance and shape. In particular, Mitchell et al. [2] introduced a multistage hybrid active appearance model (AAM) combined with the gradient information for segmenting MR images of the heart. Lin et al. [3] proposed an automatic framework to segment the left and right ventricular inner (endocardium) and outer (epicardium) borders in CMR images using a simple contour detection method combined with temporal Fourier analysis of image cines. A variational framework by Paragios [4] combined the boundary- and region-based LV segmentation in the CMR images by using a geodesic active region (GAR) model. To obtain a more accurate automatic level set-based segmentation of the rat CMR images, Pluemp et al. [5] added an elliptic shape prior of the heart to probabilistic region- and edge-based information.

Recently, an automatic approach by Kurkure et al. [6] combined intensity- and texture-based fuzzy affinity maps with dynamic-programming-based boundary detection to segment the myocardial contours in CMR images. A semi-automated framework by Li et al. [7], tested on CT, perfusion MR, and cine CMR images, exploits two different energy functionals, derived from a dual "object-background" intensity model and a shape prior, for segmenting myocardial borders. Mahapatra and Sun [8] used Markov random field (MRF) based graph cut optimization to segment the LV borders from perfusion CMR images.

However, the segmentation in most of the known frameworks is not sufficiently accurate and reliable because image intensities for the goal objects and their background vary much across subjects and time, parametric shape models become unsuitable for discontinuous objects due to a small number of distinct cardiac landmarks, and deformable models without adequate appearance and shape priors fail under excessive image noise, poor resolution, or diffuse boundaries.

After segmenting the borders, the wall thickening is assessed by automated or semi-automated wall thickness measurement techniques (e.g., [9]). The measurements often exploit the centerline algorithm [10] to determine planar distances between the inner and outer borders for each image. However, these methods are typically sensitive to the contours' imperfections, subject to errors in case of noisy images or broken and irregular boundaries, and still require a search method to co-locate the corresponding borders' points. Recently, Prasad et al. [11] proposed to measure myocardial thickening more reliably by solving a partial differential Laplace equation. However, their approach was based on manual editing of the segmented contours by a cardiologist, i.e., was prone to the inter-observer variability, and did not address the one-pixel distance scenario where both the inner and outer contours share common pixels.

We propose below an automatic framework to analyze cine CMR images that overcomes the aforementioned limitations. The myocardial contours are segmented from surrounding tissues with a geometric deformable model guided by a stochastic speed function [12] that accounts for a shape prior and features of image intensity and spatial interaction. These features are integrated with a two-level joint Markov-Gibbs random field (MGRF) model of the LV and background (Fig. 1). The wall thickness is accurately measured on the basis of point-to-point correspondences between the LV wall borders found by solving the Laplace equation. Then, the calculated wall thickening values are refined using their 3-D Gauss-Markov random field model and MAP estimates.

2. MYOCARDIAL BORDERS SEGMENTATION

This stage exploits a powerful level set-based deformable model, which is very popular in today's medical image analysis due to the

*Corresponding author:- Tel:(502)-852-5092, Fax:(502)-852-6806, E-mail: aselba01@louisville.edu

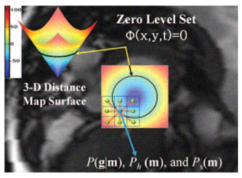

Fig. 1. Integrating image features for level set evolution.

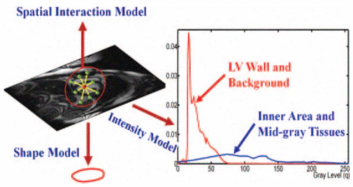

Fig. 2. Aligning a joint MGRF model to a shape prior.

flexibility of an evolving contour on the xy-plane and the lack of need for parametrization. The object-background boundary at each moment t is represented by a zero level $\phi_t(x,y) = 0$ of an implicit level set function, namely, a distance map $\phi_t(x,y)$ containing the signed minimum Euclidean distances from every point (x,y) to the boundary (negative for the interior and positive for the exterior points). The distance map is evolved iteratively [13], the evolution being guided by a speed function $V_n(x,y)$:

$$\phi_{n+1}(x,y) = \phi_n(x,y) - \tau V_n(x,y)|\nabla\phi_n(x,y)| \qquad (1)$$

where n indicates the time instant $t = n\tau$ (taken with a step $\tau > 0$) and $\nabla\phi_n = [\frac{\partial\phi_n}{\partial x}, \frac{\partial\phi_n}{\partial y}]$ is the gradient of $\phi_n(x,y)$.

Joint MGRF Model of an LV and Background: Let $\mathbf{Q}$ and $\mathbf{L} = \{0,1\}$ be a set of integer gray values and a binary set of object ("1") and background ("0") labels, respectively. Let $\mathbf{R}$ denote a 2-D arithmetic lattice supporting a given grayscale image $\mathbf{g} : \mathbf{R} \to \mathbf{Q}$ to be segmented (co-aligned to a shape prior, Fig. 2), and its goal binary "object-background" region map $\mathbf{m} : \mathbf{R} \to \mathbf{L}$. The image $\mathbf{g}$ and its map $\mathbf{m}$ are described with a joint probability model $P(\mathbf{g},\mathbf{m}) = P(\mathbf{g}|\mathbf{m})P(\mathbf{m})$ combining a 2^{nd}-order MGRF $P(\mathbf{m})$ of region labels and a conditionally independent random field $P(\mathbf{g}|\mathbf{m})$ of image intensities given the map. The map model $P(\mathbf{m}) = P_{\rm s}(\mathbf{m})P_{\rm h}(\mathbf{m})$ has two parts: a shape prior probability $P_{\rm s}(\mathbf{m})$ for a set of co-aligned training maps, and a 2^{nd}-order MGRF model $P_{\rm h}(\mathbf{m})$ of a spatially homogeneous evolving map.

Shape Model: The shape prior probability is specified with a spatially variant independent random field of region labels $P_{\rm s}(\mathbf{m}) = \prod_{(x,y)\in\mathbf{R}} p_{{\rm s}:x,y}(m_{x,y})$; where the factors are the empirical pixel-wise object, $p_{{\rm s}:x,y}(1)$, and background, $p_{{\rm s}:x,y}(0) = 1 - p_{{\rm s}:x,y}(1)$, probabilities, respectively, for the manually segmented training images co-aligned by a rigid 2-D transformation. Our framework exploits three shape priors (built at the learning stage from different subjects) for the basal, mid-cavity and apical levels. Figure 3 illustrates the process of building the inner and outer shape priors for the mid-cavity level. The CMR images from the training set are co-aligned by a rigid 2-D transformation maximizing their mutual information (MI) [14]. The inner and outer areas are manually segmented by a medical imaging expert, and their pixel-wise object prior probabilities $p_{{\rm s}:x,y}(1)$ are estimated by counting the frequencies of occurrence of the pixel (x,y) in the inner or outer area of the LV, respectively (Fig. 4).

Intensity Model: Just as in [15], specific visual appearance of the LV in each data set to be segmented is taken into account by modeling a marginal gray level distribution within each current evolving boundary with a linear combination of discrete Gaussians (LCDG). Close approximation with LCDG separates each factor of the joint empirical gray level distribution, $P(\mathbf{g}) = \prod_{(x,y)\in\mathbf{R}} p_{\rm mix}(g_{x,y})$, into two (object and background) components, $(p(q|\lambda) : q \in \mathbf{Q}); \lambda \in \mathbf{L}$. The LCDG modeling restores transitions between these components more accurately than conventional mixtures of only positive Gaussians, thus yielding a better initial region map formed by pixel-wise classification of the image gray values.

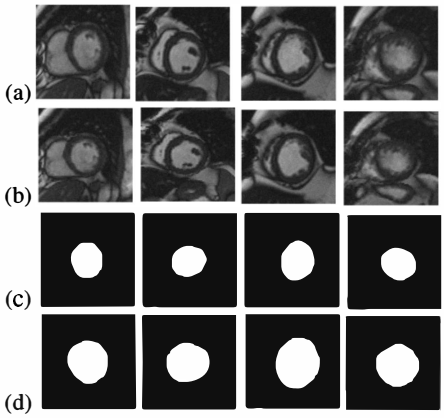

Fig. 3. Forming the shape priors: (a) training samples; (b) their affine MI-based alignment, and manually segmented inner (c) and outer (d) regions.

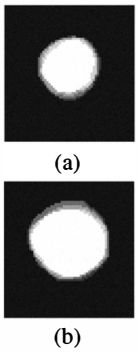

Fig. 4. Gray-coded inner (a) and outer (b) shape priors.

Spatial Interaction Model: For a smoother level set evolution and more accurate segmentation, spatially homogeneous interactions between the region labels are modeled with the popular Potts model (the MGRF with the nearest 8-pixel neighborhood) having bi-valued Gibbs potentials (Fig. 2), depending only on whether the nearest pairs of labels are equal or not. Let $f_{\rm eq}(\mathbf{m})$ denote the relative frequency of equal labels in the neighboring pixel pairs $\{(x,y),(x+\xi,y+\eta)\} \in \mathbf{R}^2; (\xi,\eta) \in \{(\pm1,0),(0,\pm1),(\pm1,\pm1)\}$. The initial region map (obtained by the pixel-wise classification) results in the approximate analytical estimates of the potentials (see e.g., [16]): $V_{\rm eq} = -V_{\rm ne} = 4f_{\rm eq}(\mathbf{m}) - 2$ that allow for computing the pixel-wise probabilities $p_{{\rm h}:x,y}(m_{x,y})$ of the labels, $m_{x,y} = \lambda; \lambda \in \mathbf{L}$ at each step of the contour evolution.

Stochastic Speed Function: Let κ be the mean contour curvature and let $\vartheta(x,y)$ specify the evolution magnitude and direction at the contour point (x,y). The stochastic speed function in Eq. (1) is defined as [12] : $V(x,y) = \kappa\vartheta(x,y)$; where

$$\vartheta(x,y) = \begin{cases} -P_{1:x,y} & \text{if} \quad P_{1:x,y} > P_{0:x,y} \\ P_{0:x,y} & \text{otherwise} \end{cases} \qquad (2)$$

Here, $P_{1:x,y} = \frac{\Omega_{1:x,y}}{\Omega_{1:x,y}+\Omega_{0:x,y}}$ and $P_{0:x,y} = 1 - P_{1:x,y}$; where

$$\begin{aligned} \Omega_{1:x,y} &= p(q|1)p_{{\rm h}:x,y}(1)p_{{\rm s}:x,y}(1) \\ \Omega_{0:x,y} &= p(q|0)\,(1 - p_{{\rm h}:x,y}(1))\,(1 - p_{{\rm s}:x,y}(1)) \end{aligned}$$

and $p_{{\rm h}:x,y}(1)$ is the probability of the object label at the pixel (x,y) in the Potts model $P(\mathbf{m})$ at the current evolution step.

3. WALL THICKNESS ANALYSIS

Wall thickening, i.e., changes in wall thickness during the cardiac cycle, is a popular and well-documented local index that characterizes the integrated physiology of a patient. The wall thickness is measured using the Euclidean distance between two corresponding points located on the inner and outer borders. In this paper, the correspondences, or matches, between the borders' points are found by solving, in the segmented wall, the Laplace equation for a scalar potential field Ψ:

$$\nabla^2\Psi = \frac{\partial^2\Psi}{\partial x^2} + \frac{\partial^2\Psi}{\partial y^2} = 0 \qquad (3)$$

Generally, the solution of the Laplace equation between two boundaries, such as $\mathbf{P_A}$ and $\mathbf{P_B}$ in Fig. 5, results in intermediate equipotential surfaces (dashed lines in Fig. 5) and streamlines that connect both the boundaries. The streamlines (e.g., the line connecting the points P_{ai} and P_{bj} in Fig. 5) are orthogonal to all the equipotential surfaces and establish the point-to-point correspondences between the boundaries.

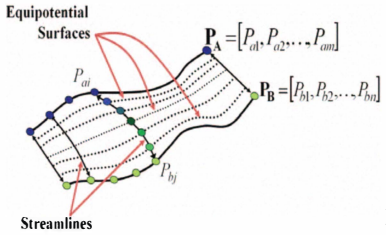

Fig. 5. 2-D correspondences by a potential field.

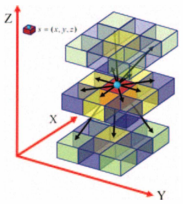

Fig. 6. Pairwise voxel interaction in a 3-D GGMRF image model.

Physiological Parameter (Wall Thickening, δ) Estimation: For each image section k, we calculated the wall thickness changes, $\delta_k = W_{ES} - W_{ED}$, between the wall thickness values W_{ES} and W_{ED}, corresponding to the end systolic volume (the smallest inner area volume) and end diastolic volume (the greatest inner area volume), respectively. For continuity preservation and inconsistencies removal (i.e., smoothed δ), the δ_k values are modeled with a generalized 3-D Gauss-Markov random field (GGMRF) [17] with the 26-neighborhood voxel shown in Fig. 6. For each patient, the δ_k values in all image sections were used to build a 3-D model of the LV. The continuity of the wall thickening values in the constructed 3-D volume is preserved by estimating its maximum *a posteriori* (MAP) estimate as shown in [17]:

$$\hat{\delta}_s = \arg\min_{\tilde{\delta}_s} \left\{ \left| \delta_s - \tilde{\delta}_s \right|^{\alpha} + \sigma^{\alpha} \lambda^{\beta} \sum_{r \in \nu_s} \eta_{s,r} \left| \tilde{\delta}_s - \delta_r \right|^{\beta} \right\}$$

where δ_s and $\tilde{\delta}_s$ are thickening values at the observed 3-D location $s = (x, y, z)$ and its neighbors from the 26-neighborhood voxel set ν_s in Fig. 6, respectively; $\eta_{s,r}$ is the GGMRF potential, σ and λ are scaling factors; $\beta \in [1.01, 2.0]$ controls the smoothing (e.g., smooth, $\beta = 2$, vs. relatively abrupt edges, $\beta = 1.01$); and $\alpha \in [1, 2]$ determines the Gaussian, $\alpha = 2$, or Laplace, $\alpha = 1$, prior distribution of the MAP estimator.

4. EXPERIMENTAL RESULTS

The proposed framework has been tested on 3-D cine CMR images collected as time series (consisting each of 25 frames of the same image section) through the cardiac cycle for 26 independent data sets for subjects undergoing cardiac stem cell therapy for end-stage heart disease after heart attack. Some results of segmenting the LV wall borders on the test cine CMR images for four subjects together with the errors comparing them to the manual segmentation by an expert are shown in Fig. 7.

Figure 8 illustrates the process of determining the wall thickness from the point-to-point border correspondences on the segmented cine CMR images. For visual assessment, the wall thickening is displayed as pixel-wise parametric color-coded maps that characterize the physiological data. To visualize the color maps, the wall

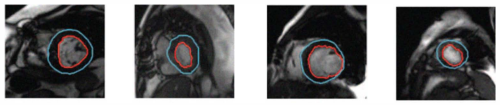

e_{inn}	0.15%	0.11%	0.13%	0.08%
e_{out}	0.08%	0.13%	0.05%	0.15%

Fig. 7. Segmentation errors for the inner (e_{inn}; red) and outer (e_{out}; cyan) borders with respect to the manual tracing.

thickening values are normalized by relating them to the maximum wall thickening measured in all image sections for both the pre- and post-treatments. To quantify the wall thickening measurement, the estimated wall thickening values are assessed using the standardized myocardial segments model [18] in which the LV wall is divided into 17 circumferential segments (Fig. 9).

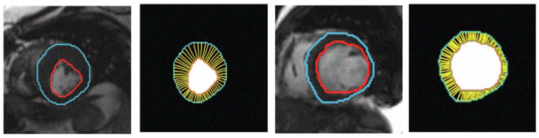

(a) (b) (c) (d)

Fig. 8. Typical cine CMR images (a, c) with inner (red) and outer (cyan) borders, and the associated streamlines (b, d) obtained by solving the Laplace equation.

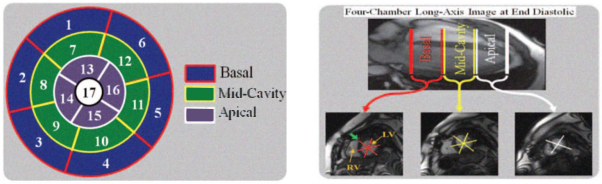

(a) (b)

Fig. 9. The myocardial 17-segment model [18]:(a) circumferential polar plot and (b) locations of segments for basal (left), mid-cavity (middle), and apical (right) image sections. The segment numbering starts counter-clockwise from the anatomical landmark indicated by the green arrow in the basal section.

Figure 10 presents parametric maps of the wall thickening over multiple image sections before and after the 3-D GGMRF smoothing for pre- and post-treatments for one of the subjects involved in our cardiac stem cell therapy project. Table 1 summarizes the average wall thickening values, $\bar{\delta}$, for each of the 17 segments corresponding to the color maps shown in Fig. 10.

5. CONCLUSIONS

Ventriculometry based on finding the inner and outer myocardial boundaries results in well-established and documented parameters, such as wall thickening, end diastolic and end systolic volumes, and ejection fraction. The proposed framework determines these parameters automatically by accurate segmentation of myocardial inner and outer borders in cine CMR images and accurate searching for corresponding points on the myocardial borders. In our initial experiments, this approach has been applied to the cine CMR images for subjects undergoing cardiac stem cell therapy for end stage heart disease after heart attack. The tentative agreement between our measurements and other clinical indexes of the LV (e.g., ejection fraction) is very promising and indicates good potential for future clinical applications of the proposed approach.

Table 1. Average wall thickening, $\bar{\delta}$ (mm), for the 17-segment model [18] for the results shown in Fig. 10. 'IMP' stands for improvement.

Section#	1	2	3	4	5	6	7	8	9	10	11	12	13	14	15	16	17
Pre	5.39	3.32	1.44	2.75	4.98	4.62	4.83	2.17	2.15	1.64	3.03	5.82	2.97	2.79	1.73	3.40	0.00
Post	7.10	4.21	1.86	5.90	5.33	6.88	5.55	2.41	2.25	1.73	3.65	7.22	3.86	3.24	2.86	4.50	0.00
IMP %	31.7	26.8	29.2	112	7.03	48.9	14.9	11.1	4.65	5.49	20.5	24.1	29.9	16.1	65.3	32.4	0.00

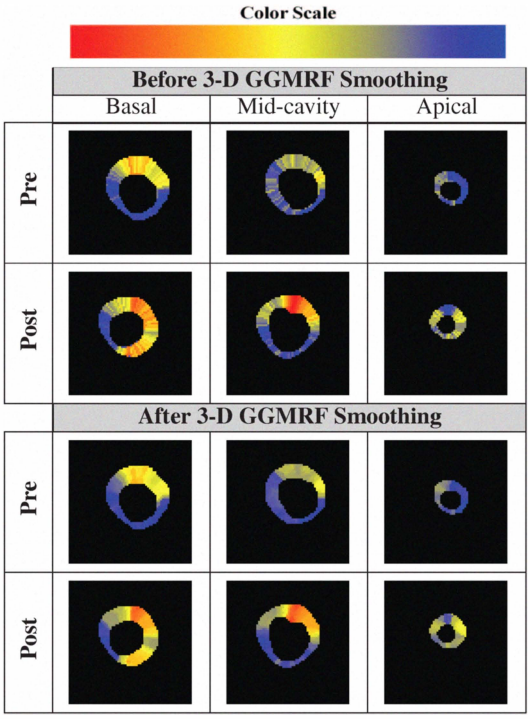

Fig. 10. Color-coded maps for the changes of wall thickness for a pre- and post-treatment test data set before and after the 3-D GGMRF smoothing with $\sigma = 1$, $\lambda = 5$, $\beta = 1.01$, $\alpha = 2$, and $\eta_{s,r} = \sqrt{2}$. The red and blue ends of the color scale relate to the maximum and minimum thickness, respectively.

6. REFERENCES

[1] G. Beache, V. Wedeen, and R. Dinsmore, "Magnetic resonance imaging evaluation of left ventricular dimensions and function and pericardial and myocardial disease," *Coronary Artery Disease,* vol. 4, no. 4, pp. 328–333, 1993.

[2] S. Mitchell, H. Bosch, B. Lelieveldt, R. van der Geest, et al., "Multistage hybrid active appearance model matching: Segmentation of left ventricles in cardiac MR images," *IEEE Trans. Med. Imag.,* vol. 20, no. 5, pp. 415–423, 2001.

[3] X. Lin, B. Cowan, and A. Young, "Automatic detection of left ventricle in 4D MR images: Experience from a large study," in *Proc. Int. Conf. Medical Image Computing and Computer-Assisted Intervention (MICCAI'06),* Copenhagen, Denmark, October 1–6, 2006, vol. 1, pp. 728-735.

[4] N. Paragios, "A variational approach for the segmentation of the left ventricle in MR cardiac images," *Int. J. Comput. Vis.,* vol. 50, no. 3, pp. 345–362, 2002.

[5] C. Pluempitiwiriyawej, J. F. Moura, Y.-J. Wu, and C. Ho, "STACS: New active contour scheme for cardiac MR image segmentation," *IEEE Trans. Med. Imag.,* vol. 24, no. 5, pp. 1360–1370, 2005.

[6] U. Kurkure, A. Pednekar, R. Muthupillai, S. Flamm, and I. Kakadiaris., "Localization and segmentation of left ventricle in cardiac cine-MR images," *IEEE Trans. Biomed. Eng.,* vol. 56, no. 5, pp. 1179–1191, 2009.

[7] C. Li, X. Jia and Y. Sun, "Improved semi-automated segmentation of cardiac CT and MR images," in *Proc. IEEE Int. Sym. Biomedical Imaging: from Nano to Micro (ISBI'09),* Boston, MA, June 28- July 1, 2009, pp. 25–28.

[8] D. Mahapatra and Y. Sun, "Joint registration and segmentation of dynamic cardiac perfusion images using MRFs," in *Proc. Int. Conf. Medical Image Computing and Computer-Assisted Intervention (MICCAI'10),* Beijing, China, September 20–24, 2010, vol. 1, pp. 493–501.

[9] N. Beohar, J. D. Flaherty, C. J. Davidson, M. I. Vidovich, et al., "Quantitative assessment of regional left ventricular function with cardiac MRI: Three-dimensional centersurface method," *Catheterization and Cardiovascular Interventions,* vol. 69, pp. 721–728, 2007.

[10] F. H. Sheehan, E. L. Bolson, H. T. Dodge, D. G. Mathey, et al., "Advantages and applications of the centerline method for characterizing regional ventricular function," *Circulation*, vol. 74, no. 2, pp. 293-305, 1986.

[11] M. Prasad, A. Ramesh, P. Kavanagh, J. Gerlach, et al., "Myocardial wall thickening from gated Magnetic Resonance images using Laplace's equation," in *Proc. SPIE, Medical Imaging 2009: Computer-Aided Diagnosis,* Lake Buena Vista, FL, USA, February 2009, vol. 7260, pp. 21–28.

[12] F. Khalifa, A. El-Baz, G. Gimelfarb, R. Ouseph, and M. Abo El-Ghar, "Shape-appearance guided level-set deformable model for image segmentation," in *Proc. IEEE Int. Conf. Pattern Recogn. (ICPR'10),* Istanbul, Turkey, August 23–26, 2010, pp. 4581–4584.

[13] S. Osher and R. Fedkiw, *Level Set Methods and Dynamic Implicit Surfaces* (*Applied Mathematical Sciences*, vol. 153), Springer, 2006.

[14] P. Viola, and W. M. Wells III, "Alignment by maximization of mutual information," *Int. J. Comput. Vis.,* vol. 24, no. 2, pp. 137–154, 1997.

[15] A. El-Baz and G. Gimel'farb, "EM Based approximation of empirical distributions with linear combinations of discrete Gaussians," in *Proc. IEEE Int. Conf. Image Process. (ICIP'07), San Antonio, Texas, USA,* September 16–19, 2007, vol. 4, pp. 373–376.

[16] A. Farag, A. El-Baz, and G. Gimel'farb, "Precise segmentation of multimodal images," *IEEE Trans. Image Process.,* vol. 15, no. 4, pp. 952–968, 2006.

[17] C. Bouman and K. Sauer, "A generalized Gaussian image model for edge-preserving MAP estimation," *IEEE Trans. Image Process.,* vol. 2, no. 3, pp. 296–310, 1993.

[18] M. Cerqueira, N. Weissman, V. Dilsizian, A. Jacobs, et al.,"Standardized myocardial segmentation and nomenclature for tomographic imaging of the heart: A statement for healthcare professionals from the cardiac imaging committee of the council on clinical cardiology of the american heart association" *Circulation,* vol. 105, pp. 539–542, 2002.